Patient to model framework for biomechanical simulations

Project Number:	FP7--IST-*223979*
Deliverable id:	D6.1
Deliverable name:	Patient to model framework for biomechanical simulations
Submission Date:	30/06/2009

COVER AND CONTROL PAGE OF DOCUMENT	
Project Acronym:	CONTRA CANCRUM
Project Full Name:	Clinically Oriented Translational Cancer Multilevel Modelling
Document id:	D6.1
Document name:	Patient to model framework for biomechanical simulations
Document type (PU, INT, RE)	RE
Version:	1
Submission date:	30/06/2009
Editor: Organisation: Email:	Thibaut Bardyn, Philippe Büchler UNIBE thibaut.bardyn@artorg.unibe.ch

Document type PU = public, INT = internal, RE = restricted

ABSTRACT:

D6.1 Patient to model framework for biomechanical simulations, Report on the automatic generation of patient-specific models for the simulation of cancer biomechanics (produced by T6.1). Final version delivered in PM10 (end of June 2009), after early drafts circulated within consortium...

KEYWORD LIST: finite element, automatic, patient-specific, smoothing

MODIFICATION CONTROL			
Version	Date	Status	Author
1.0	29/06/09	Template	Thibaut Bardyn
2.0		Draft	
3.0		Draft	

List of Contributors

- Thibaut Bardyn, University of Bern
- Philippe Büchler, University of Bern
- Mauricio Reyes, University of Bern
- Name, Institute

Contents

Executive Summary

The ContraCancrum, i.e. the Clinically Oriented Translational Cancer Multilevel Modelling, project aims at developing a composite multilevel platform for simulating malignant tumour development and tumour and normal tissue response to therapeutic modalities and treatment schedules.

The project aims at having an impact primarily in (a) a better understanding of the natural phenomenon of cancer at different levels of biocomplexity and, most importantly, (b) a disease treatment optimization procedure in the patient's individualized context by simulating the response to various therapeutic regimens. The predictions of the simulators to be developed will rely on the imaging, histopathological, molecular and clinical data of the patient. Fundamental biological mechanisms involved in tumour development and tumour and normal tissue treatment response such as metabolism, cell cycle, tissue mechanics, cell survival following treatment etc. will be modelled. Stem cells will be addressed in the context of both tumour and normal tissue behaviour. From a mathematical point of view, the simulators will exploit several discrete and continuous mathematics methods such as cellular automata, the generic Monte Carlo technique, finite elements, differential equations, novel dedicated algorithms etc. A study of the analogies of tumour growth with embryological development is expected to provide insights into both mechanisms.

ContraCancrum will deploy two important clinical studies for validating the models, one on lung cancer and one on gliomas. The crucial validation work will be based on comparing the multi-level therapy simulation predictions with the actual medical data (including medical images), acquired before and after therapy.

ContraCancrum aims to pave the way for translating clinically validated multilevel cancer models into clinical practice.

This deliverable presents the first milestone for the biomechanical simulation of tumour development. The method used to automatically generate the mesh for the finite element analysis is introduced and assessed. Examples of the application of the algorithm on brain models are also presented. This work is strongly linked with the segmentation provided by the WP7 and the cellular simulator provided by the WP4.

The innovative oncosimulator that will be developed in the framework of the Contra Cancrum European project combines a biomechanical and a cellular model. The biomechanical simulation aims at calculating the mechanical state in the anatomy around the tumour during its growth. This mechanical information is then transferred to the cellular simulator which will predict the behaviour of the cells within this tumour.

The first step when building a biomechanical model is to generate a finite element mesh on which various conditions will then be set. The clinical orientation of the oncosimulator implies this mesh generation to be fully automatic and fast. The following report presents the steps that led to an adapted method.

1 Scientific background and previous work

1.1 Finite element analysis

Finite element analysis[1] (FEA) has been used for almost thirty years in the field of biomechanics on applications as various as design of medical devices, surgery simulation or the prediction of surgical outcome. Finite element models allow to solve complex partial differential equations via the discretization of space into a finite number of small elements. The discrete value of a field (displacement, temperature, fluid, velocities,…) in a body when it is submitted to boundary conditions is calculated. The body is divided into basic shapes called elements. The accuracy of the finite element simulation depends on the number but also on the shape and type of elements used (figure 1). Elements are interconnected at points called nodes. In the framework of the ContraCancrum project, displacement, stresses and strains in the tissue are calculated during the evolution of the tumour. In this particular case, the governing equations relating force to displacement for each element are formulated and assembled to give a collection of equations. These equations describe the behaviour of the elements and hence the behaviour of the body. The set of equations takes the following matrix form:

$$\mathrm{F} = [\mathrm{K}]\mathrm{U} \qquad (1)$$

Where $[K]$ is the stiffness matrix describing the mechanical properties of the material. F is the vector of nodal forces (the boundary conditions on the model) and U is a vector of displacements also defined on the nodes of the model. Solving the finite element analysis consists in inverting $[K]$ and multiplying it with F which will give U. Stresses and strains can then be calculated from the displacement obtained. In case of nonlinear material such as soft tissues, or when large deformations occur, the stiffness matrix depends on the displacement and consequently the solution of the problem can become highly complex.

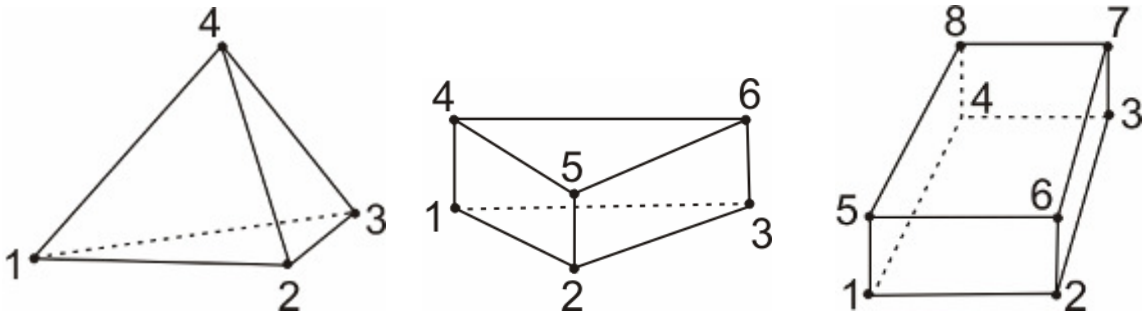

Fig. 1. Example of specific elements used in the finite element method with their node numbering. From left to right: tetrahedron, prism and hexahedron elements. The hexahedron element is known as the most accurate of all three types of elements.

In the field of tumour biomechanics, finite element analysis has been used first to evaluate deformation of the surrounding tissues due to the tumour at a specific state[2,3,4]. Further studies have then aimed at predicting the growth of the tumour. First a 2D model was proposed which allowed to calculate stresses in the surrounding tissues[5]. A more advanced 3D model including diffusion of cancerous cells within normal tissue has recently been developed by Clatz[6].

1.2 Patient-specific mesh

Finite element analyses for which geometrical and material information are adapted to a patient belong to the category of patient-specific finite element analyses. The main drawback of this technique as compared to a more generic method is the creation of a model that fits to the patient morphological and physiological features. Usually, the creation of a patient-specific model is divided into the following steps:

- A CT scan or MRI of a patient is acquired and segmented using either automatic or manual methods. This segmentation leads to a three-dimensional reconstruction of patient anatomy. The 3D model obtained is meshed and leads to a patient-specific finite element mesh. This procedure has to be fast, accurate, robust and general [7]. The degree of automation of segmentation and meshing defines their clinical usefulness. Several algorithms exist for the automatic creation of a mesh but none verify the requirements imposed by a clinical application [8].
- If possible, patient-specific mechanical properties are assigned to the mesh. In the case of the bone, inhomogeneous properties can be retrieved from voxel intensities in the CT scan[9]. In the case of the brain, patient-specific information about the direction of the fibers can be retrieved from DT MRI. For the remaining parameters, generic mechanical properties retrieved from *in vitro* experiments have to be used.
- Standard load cases are applied on the model which is then solved, giving a patient-specific mechanical state of the anatomy. In the case of *in vitro* experiments, the loads applied are similar to those used in the mechanical setup that tests the structure.

A number of softwares dedicated to the creation of subject-specific finite element models have been developped recently. Among them, Mimics (Materialise, Leuven, Belgium) and Simpleware (Simpleware Ltd., Exeter, UK) are the most popular. While Mimics offers an approach that is essentially manual, Simpleware allows to create a mesh fully automatically and to define a contact law between the two surfaces. However, these two softwares are commercial tools and therefore are neither free nor open source.

1.3 Automatic mesh generation

The most usual way to generate a FE model consists on a series of steps using commercially software packages. Typically, a STL surface is generated from the segmented geometry which is then converted into a closed volume that can then be meshed. In addition to the several software packages needed, the process is very time consuming and can hardly be automatized. The resulting mesh is highly dependent on the quality of the surface STL, the STL being an assembly of triangular faces and the final FE mesh is also limited to tetrahedrons (therefore limiting meshing possibilities). This process is extremely long and tedious and the trend for patient-specific finite element study has increased the need for automatic mesh generation.

Many methods have been proposed for the automatic generation of finite element meshes[8]. The existing algorithms can be divided in three categories:

- the algorithms based on a surface mesh built from the segmentation. This surface is usually a closed polygonal simplex. The level of automation of these methods is generally low due to the processing necessary to build the surface mesh.
- the algorithms that are solely image-based. Among those is the "voxel mesh method". These algorithms are fully automated, general, and robust but lack accuracy due to jagged edges on the boundaries.
- the algorithms based on segmentation contours, such as template methods[10] or grid-based methods[11]. These algorithms sit between the two first categories in terms of accuracy, automation and robustness.

In his review paper[8], Viceconti states that none of the existing methods verifies the requirements of automation, generality, accuracy and robustness necessary for a general clinical application. Therefore, the specific needs for a clinical application have to be thoroughly analyzed in order to select the most adapted algorithm. Additionally, a balance between accuracy and processing time has also to be found.

1.4 Voxel based meshing

Keyak et al.[12,13,14] proposed a method to directly generate a mesh from a dataset of stacked images (CT scans, etc..), thus avoiding the geometric extraction step. The algorithm is referred as "voxel mesh method". In its simplest form, it transforms a voxel in the image that corresponds to the anatomy to a cubic element in the FE mesh. The resulting mesh resembles a structured "grid" of hexahedral elements. This algorithm has been widely used to generate mesh of large data such as encountered in micro CT of trabecular structure. The method is extremely robust and does not depend on the topology of the surface. Therefore, it can be adapted to any type of anatomy.

The cost of such an efficient and robust mesh construction of complex structures is a digitized approximation of curved boundaries. In the field of macroscopic biomechanics, the inexact boundary representation characteristic of digital FE models produces higher local solution errors as compared to traditional smooth boundary models. Other authors have also reported oscillations of voxel meshes accuracy with successive refinement near the domain boundaries[15]. Moreover, it was shown that results were highly sensitive to the element size.

For this reason, smoothing of the surface was introduced to improve accuracy of the voxel meshes. Studies showed significant improvements on basic examples[16] and anatomical structure[17].

1.5 Surface smoothing

Automatically generated meshes such as produced by "voxel mesh" method bear inaccurate surfaces. This may induce computational inaccuracies since boundary conditions are set on the external or internal envelope of the mesh. Improving the external aspect of a mesh is possible using surface smoothing. Surface smoothing redistributes the vertices without changing the connectivity (and thus is particularly adapted to finite element). As the simplest and most straightforward method, Laplacian smoothing relocates the vertex position at the average of the nodes connecting to it [18]. Although extremely efficient in terms of computation, the process results in surface shrinkage which can have a high impact on FE predicted mechanics. To cope with this limitation, several authors proposed an improved Laplacian smoothing algorithm to prevent surface shrinkage. Taubin smoothing and mean curvature flow are among the most popular of these methods[19].

Later on, Taubin proposed an innovative approach to the problem of surface smoothing: the geometric signal processing. The method consists in generating the Fourier decomposition of the surface and to apply a low-pass filter to the three-dimensional signal[20]. The method prevents surface shrinkage but also maintains the main geometric features of the surface.

The downside of surface smoothing as applied to finite element mesh is the generation of ill-conditioned elements on the surface due to excessive deformations. Therefore, surface smoothing is often combined with a mesh untangling method or interior mesh smoothing[21]. Mesh untangling consists in removing inverted elements with a negative volume (or jacobian). Interior mesh smoothing aims at improving the general quality of the elements. This is usually done via optimization procedures which can be computationally expensive. In general, degree of smoothing is limited to limit the number of distorted elements generated.

1.6 Objectives and structure of the report

In the present report, we propose an innovative method for the fully automatic generation of a smooth mesh. The process is fast, robust and automatic and therefore particularly adapted to a clinical application such as aimed by the Contra Cancrum project.

In the first part, the algorithms used to produce the mesh and to smooth it are presented in details. Next, an experimental study to assess the accuracy of the proposed mesh as compared to a mesh generated with a standard method is presented. Finally, the applications of the algorithm to the Contra Cancrum oncosimulator are discussed in the last part and illustrated with a few examples.

2 Automatic generation of a smooth mesh

The method chosen for the generation of a smooth mesh in the framework of the Contra Cancrum project is a combination of the "voxel mesh" with the Taubin geometric signal processing approach. Both methods were chosen because they are fast and computationally light. Moreover, it allows an easy construction of a mesh with hexahedrons which are more accurate than tetrahedral elements. An efficient and fast correction of the element quality is also proposed in the methods. The algorithms were implemented in C++ using the VTK[22] libraries which gathers a collection of visualization-oriented, open source tools.

2.1 Mesh generation

The voxel meshing method is used to generate the raw biomechanical model which will be smoothed in a second step. The input of the algorithm is the segmented image as produced by WP7. Voxels of interest in the image stack are labelled according to the anatomical structure they belong to.

The "voxel mesh" method is straightforward and associates to each labelled voxel in the stack a linear hexahedron element. The algorithm is based on a segmentation of the image and therefore result is highly dependent on the threshold chosen for the image processing. The image can be resampled to limit the number of elements in the mesh or if the size of the voxels is not isotropic (similar in every direction). In the present version of the software, numbering of the elements and the nodes is done in the reading direction of voxel. Therefore, the bandwidth of the stiffness matrix is not fully optimal and might slow down its inversion. This can be improved to reduce computational time during finite element analysis.

2.2 Smoothing

Smoothing is used to improve accuracy of the rough surfaces generated with "voxel mesh" method (figure 2 and 3). The outer surface of the mesh is extracted and smoothed according to the geometric signal processing approach of Taubin[20].

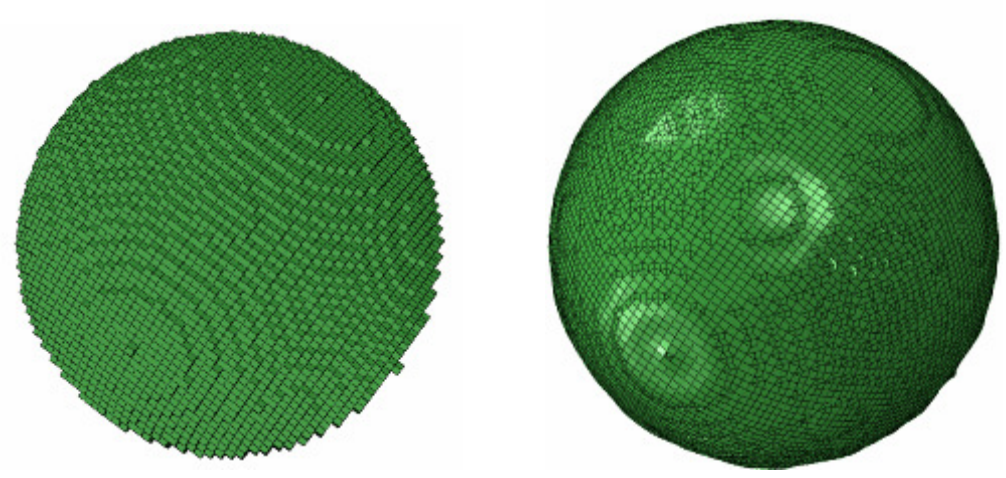

Fig. 2. Examples of the voxel mesh of a sphere (right) without smoothing and (right) enhanced with the smoothing algorithm of Taubin.

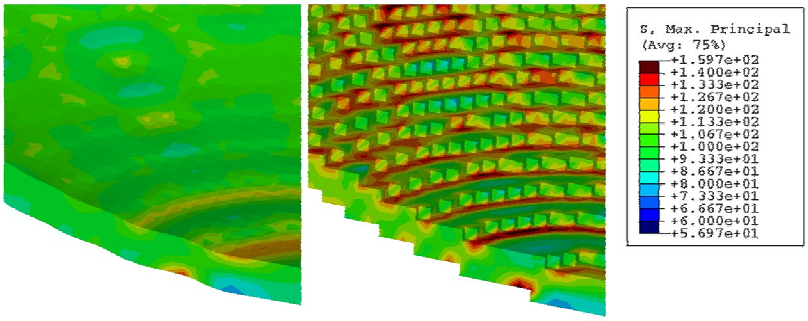

Fig. 3. Detail of a smooth (left) and non smoothed (right) sphere generated with voxel meshing. Note the even distribution of stress on the left side and the stress concentration at the corners on the right side.

The algorithm is based on a Fourier like decomposition of the geometry calculated from the laplacian operator. Let the column vector *x* be the vector of either the first, second or third coordinates of the vertices. The laplacian operator is defined on this graph signal by:

$$\Delta x_i = \sum_{j \in i^*} w_{ij} \left(x_j - x_i \right) \tag{2}$$

with i^* the neighborhood of the vertex *i* and w_{ij} the weights of the operator. The laplacian operator can be written under a matrix form

$$\Delta x = -Kx \tag{3}$$

With $K = I - W$ and $W = \left(w_{ij} \right)$ with elements equal to zero if *j* is not a neighbor of *i*. The eigenvectors e^j of the matrix *K* define the natural vibration mode of the graph and form a basis of a n-dimensional space in which the signal *x* can be decomposed as:

$$x = \sum_{j=1}^{n} \hat{x}_j e_j \tag{4}$$

This formulation is equivalent to the Discrete Fourier Transform of the signal *x*. The smoothing of the surface is then performed by applying a low pass filter with transfer function $f(K)$:

$$x' = f(K)\, x = \sum_{i=1}^{n} f(k_i)\, \hat{x}_i \cdot e_i \tag{5}$$

With $0 \le k_1 \le k_2 \le \cdots \le k_n \le 2$ the eigenvalues of the matrix *K*.

The window sync low-pass filtering transfer function is then approximated using Chebyshev polynomials:

$$T_n(w) = \begin{cases} 1 & n = 0 \\ w & n = 1 \\ 2wT_{n-1}(w) - T_{n-2}(w) & n > 1 \end{cases} \quad (6)$$

The advantages of using this approximation are that the terms of the polynomial are orthogonal, it needs few storage capacities (i.e. three-term storage), and it is numerically stable and can be defined for volume preservation purposes. The Hamming window is used as the pass-band filter (figure 4).

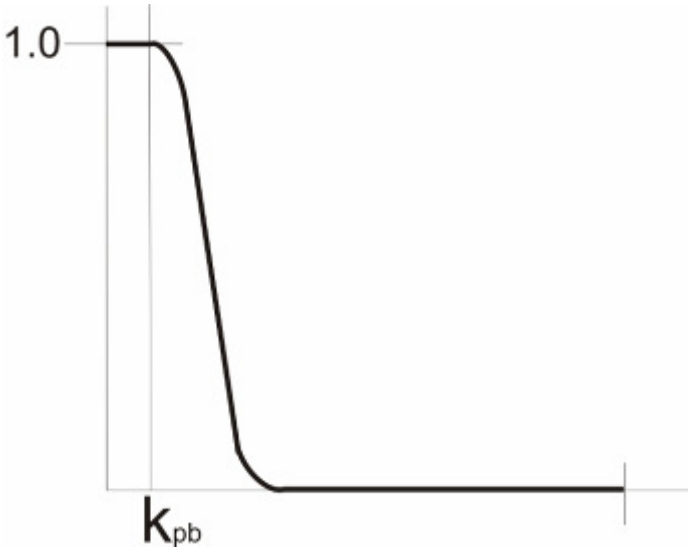

Fig. 4. Hamming window transfer function $f(k)$ used in the smoothing algorithm. The pass band frequency is here represented by k_{pb}.

The degree of smoothing (given by the value of k) is mainly limited by the fact that inverted elements might appear with extensive smoothing (figure 5).

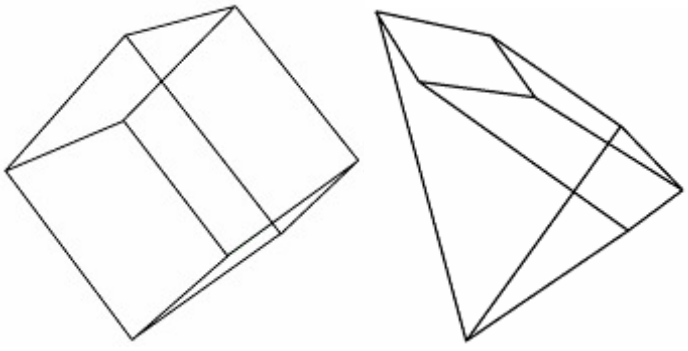

Fig. 5. Example of a distorded element (left) after excessive smoothing of the mesh. Two nodes have been pushed inwards producing. Excessive smoothing may lead to inverted elements with "negative" volume.

2.3 Improvement of the mesh quality

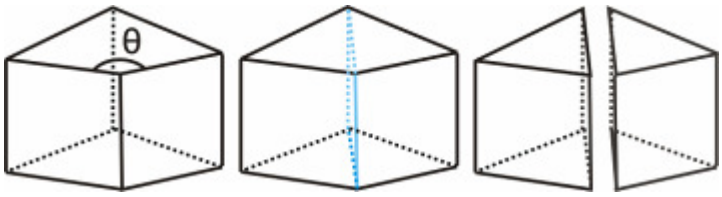

Fig. 6. Correction of elements featuring large angles (here represented by θ). The elements are divided into two prism elements along the plane that passes through the "large angle" edge.

Extensive smoothing creates distorted elements on the surface of the mesh. To improve the quality of the mesh, hexahedral elements bearing a large angle between faces are divided into prism elements (figure 6). If the angle is superior to a certain value, then the edge at the intersection of the two faces is used for the division. The element is divided by the "virtual" plane that joins this edge with its opposite in the element. This approach prevents large angle between faces of hexahedrons that produce discrepancies in the formulation of the element. Since it produced the best improvements, a threshold angle of 130 º was chosen for splitting.

2.4 Interface between tissues

Since the aim of the biomechanical model is to assess the influence of the tumour growth on the mechanics of the brain and lungs, the interface between the surrounding tissues and the tumour has to be as accurate as possible. Again, when no processing is done, voxel meshes bear jagged edges at the interface between the different structures. Therefore, smoothing has to be performed at the interface between the different tissues as well.

The smoothing algorithm used at the interface is the same as explained in section 3.2. During the segmentation, each structure is assigned a specific label. Next, the outer surface of each structure is extracted and smoothed. If this surface is also shared by another structure it is smoothed only once since high frequency components of the surface have been removed by the first smoothing.

Again, to avoid the generation of distorted elements, the correction presented in section 3.3 is used at the interface.

The algorithm was tested on two embedded sphere. Results show that the visual aspect of the sphere is significantly improved (figure 7).

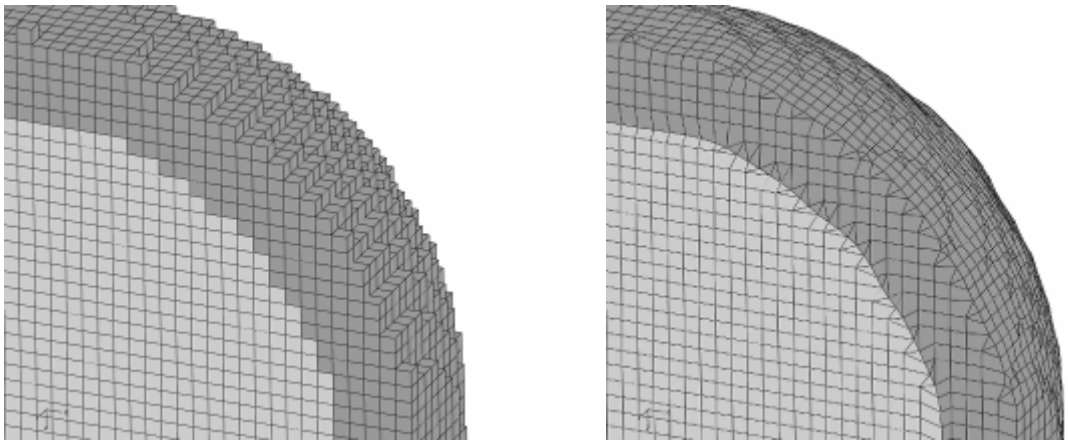

Fig. 7. Application of the smoothing on the interface between two spheres. (Left) interface without smoothing. (Right) Interface with smoothing (k=0.001) and wedge division to improve element quality.

3 Assessment of mesh accuracy

Smoothing, by removing jagged edges of the voxel mesh, should improve the accuracy of the model and allow to reach the accuracy obtained with a more standard model. The following study was therefore conducted to evaluate how much voxel mesh were improved by smoothing.

The assessment of accuracy was performed on trabecular bone model since we had access to high quality images for this structures (micro CT). CT scans of the brain or lungs were not available at the time where this report was written. Moreover, study of trabecular structure is the domain where voxel-based methods are the most widely used. It also allows to work with parameters (apparent Young's modulus in this case) which can be measured experimentally with high precision with a simple setup.

Therefore, in the present study, the influence of the degree of smoothing on the accuracy of finite element was evaluated by measuring the apparent Young's modulus of a trabecular structure. Results obtained with a reference model were compared with voxel-based models with different degrees of smoothing.

3.1 Method

The influence of the degree of smoothing on the accuracy of finite element was evaluated by measuring the apparent Young's modulus of a trabecular structure (figure 8). Results obtained with a reference model were compared with voxel-based models with different degrees of smoothing.

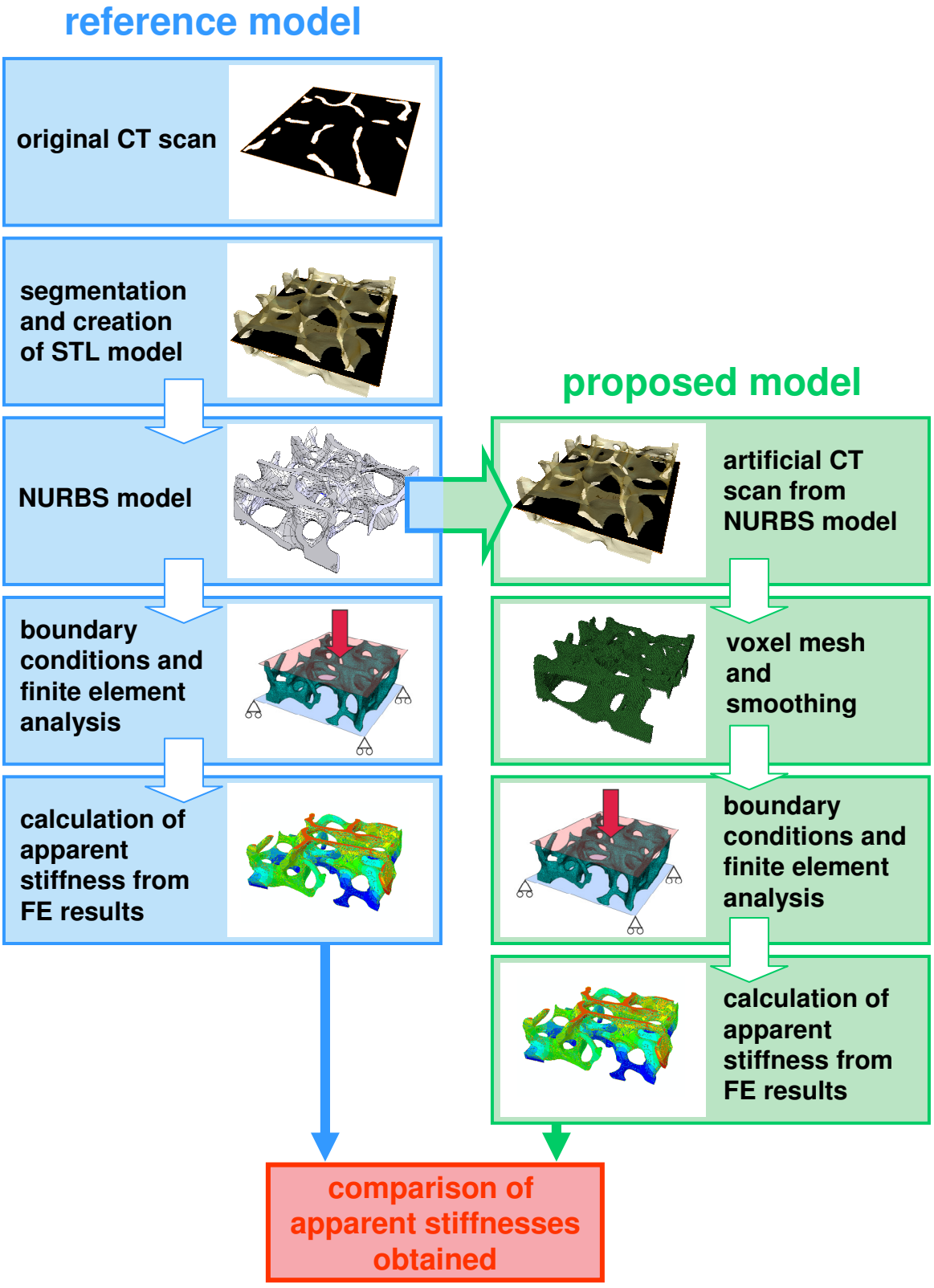

Fig. 8. Flow chart of the accuracy study. The apparent stiffness obtained with the reference model is compared with the one obtained with the proposed method.

3.1.1 Creation of the reference model

A trabecular bone specimen from human vertebra was scanned in the axial plane with a high resolution scanner (Scanco µCT40, Scanco Medical AG, Switzerland). Voxels had 8µm edges in every direction. The CT scan obtained was segmented (Amira, Visage Imaging GmbH, Germany) and an accurate 3D model with 1,286,444 triangles was generated. The triangular surface mesh of the trabecular bone was then processed further in a CAD program and fitted with a set of higher order mathematical surfaces e.g. NURBS (Non-Uniform Rational B-Splines). The smooth model of the trabecular structure obtained was considered as the reference geometry (figure 9).

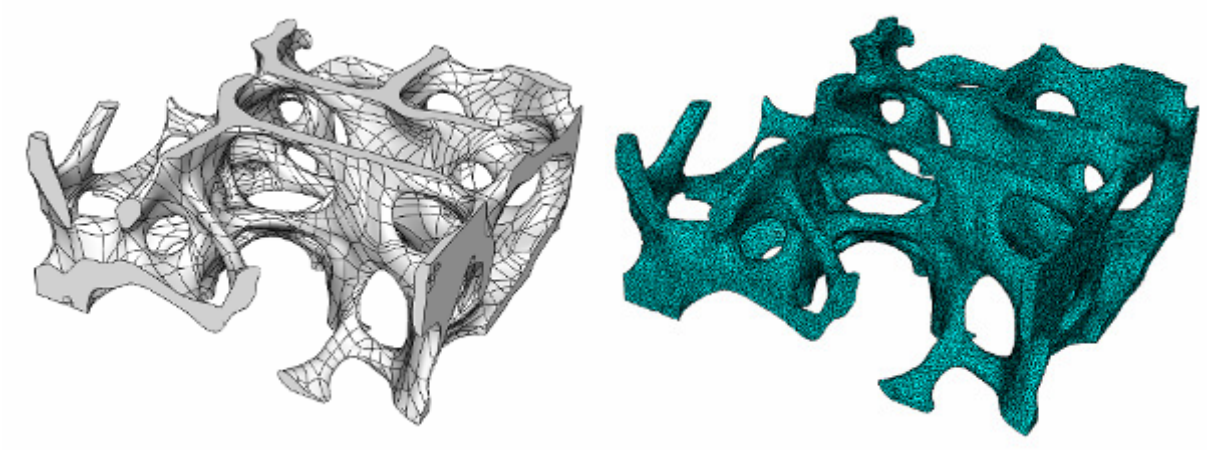

Fig. 9. (left) NURBS and (right) quadratic tetrahedral element mesh used as reference model for the study.

The NURBS model obtained was imported into a commercial finite element software (ABAQUS, Simulia, USA) and a volumetric finite element mesh with quadratic tetrahedral elements was generated. To assess for the accuracy of this reference model, a convergence study with different mesh densities was performed. Total strain energy of the mesh under an axial loading was evaluated and compared. Meshes with number of elements from 28537 to 919780 were tested. Following this convergence study, a mesh with 559814 elements quadratic tetrahedral elements was chosen as the reference model.

3.1.2 Creation of the smooth voxel-based mesh

In order to compare the reference model with voxel-based meshes, a virtual CT scan of the NURBS geometry was created using Amira. Resolution of the virtual CT scan was similar to the original one (8µm voxel size). The CT scan was resampled at voxel sizes of 16 µm, 32 µm and 64 µm producing voxel-based meshes of 231071, 29169 and 3529 elements respectively. These resolutions are typically used for *in vivo* micro CT. The method described in the second part of the report was used for the smoothing and correction of the mesh.

Smoothing was performed up to a pass-band frequency of k=0.03. Further smoothing induced negative volume elements.

Improvements in mesh quality with wedge division were measured by counting the number of distorted elements having interior angles between isoparametric lines inferior to 45 º and superior to 130 º.

3.1.3 Finite element study

Once the smoothing was performed on the voxel-based mesh, apparent Young's modulus was calculated in the three directions X, Y, Z, with Z the axis perpendicular to the axial plane of the vertebra (figure 10). A 1% strain was applied on the top of the structure while the bottom was constrained in the direction of displacement. No other faces were constrained. The apparent Young's modulus *E* was calculated according to the formula:

$$E = \frac{Fl}{\Delta u A} \qquad (4)$$

with Δu the applied displacement at the top of the structure, F the reaction force at the moving nodes, *l* the height of the sample and *A* the area as measured by the external dimensions of the cube. For all models, element material properties were assumed homogeneous and isotropic with a Young's modulus of 10GPa and a Poisson ratio of 0.3.

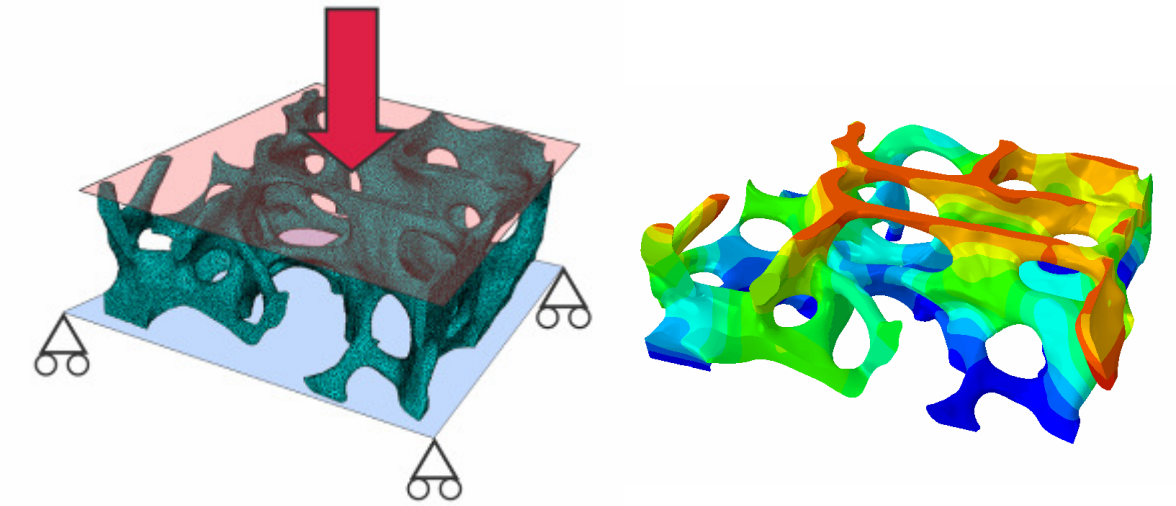

Fig. 10. (left) boundary conditions used for the assessment of the apparent Young's modulus. A prescribed displacement (read arrow) is applied on the top of the structure while the bottom is constrained not to move in the direction of the applied displacement. (right) displacement field obtained with ABAQUS red color corresponds to maximum displacement while blue color corresponds to no displacement. The Z direction displacement is represented on the present picture.

3.2 Results

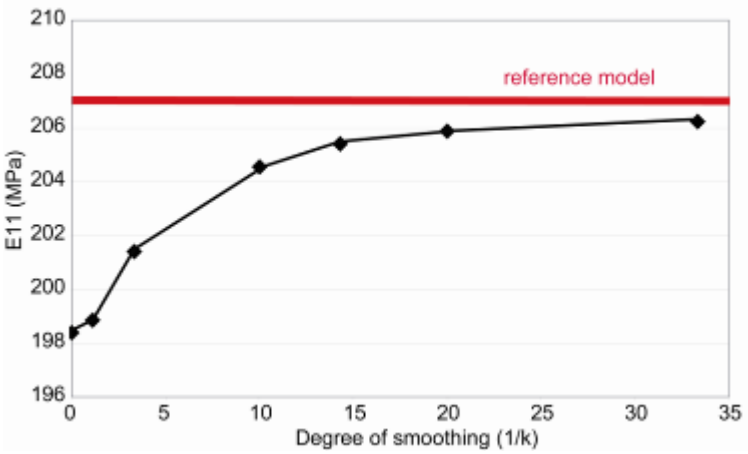

Fig. 11. Evolution of the apparent Young's modulus in the X direction for the 16µm model with different degrees of smoothing.

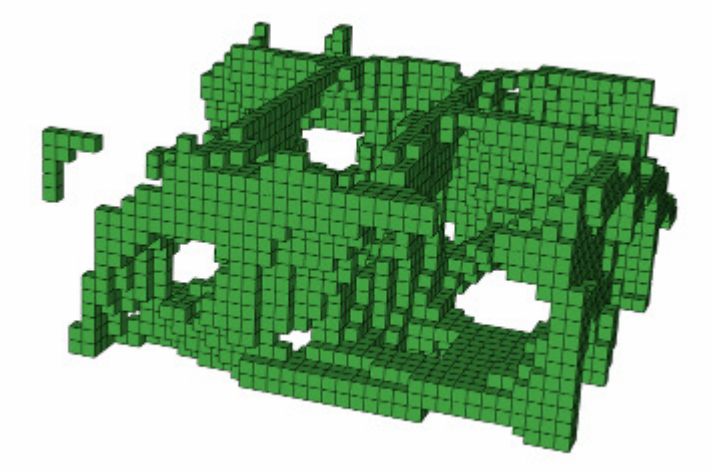

Fig. 12. Loss of trabecular connection for the 64µm model. This phenomenon explains the large error found for the apparent Young's modulus at this resolution.

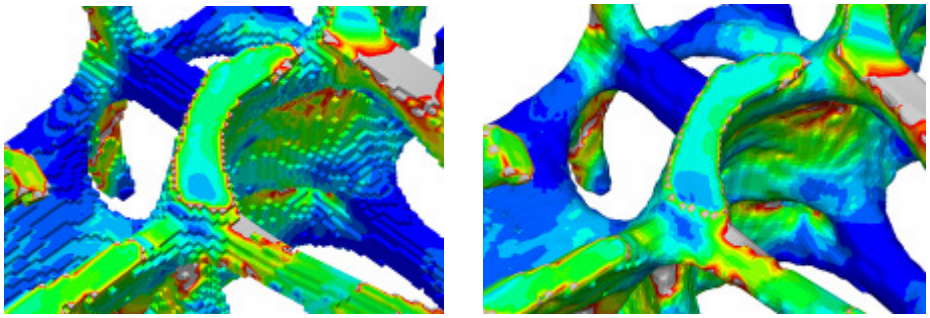

Fig. 13. Details of the Mises stress in the trabecular structure generated (left) without smoothing and (right) with smoothing.

Increasing the degree of smoothing improves the mechanical properties of the voxel-based mesh as compared to the reference model (figure 11). Smoothing improved significantly apparent Young's modulus of the voxel-based meshes for the 16 and 32µm resolutions (table 1). Improvements were not significant for the 64µm. This is due to loss of connection of the trabecular in the model (figure 12). Visually, reduction of stress concentration can be observed on the edges of the model (figure 13). The volume of the model was preserved during the smoothing and changed only by 0.02% (for k=0.03 and the 16µm model). In average, creation of the mesh and smoothing took 3 minutes for the 16 µm model on a regular 2.4GHz processor with 2.00GB of RAM.

As expected, the Young's modulus in the Z direction (≈572MPa) was found to be superior to the Young's modulus in the directions parallel to the axial plane of the vertebra (≈260 and 257MPa respectively).

Prism division significantly decreased distorted elements (table 2). However, results in terms of accuracy were not significantly changed with this improvement with an average difference of 0.19%±0.17 as compared to the model without prism division. For k=0.03, the number of elements in the 16µm was increased by 20% when prism division was used.

Table 1. Error (in % of reference value) for apparent Young's modulus between reference model and voxel-based meshes without smoothing and with maximum smoothing. Smoothing is stopped when negative volume elements are created.

	16µm			**32µm**			**64µm**		
	E11	**E22**	**E33**	**E11**	**E22**	**E33**	**E11**	**E22**	**E33**
No smoothing	4.15	3.41	5.74	8.02	15.63	10.71	12.10	33.99	23.19
K=0.03	0.36	0.97	2.17	1.32	8.67	5.19	12.25	32.37	21.44

Table 2. Comparison of the number of distorted elements generated by smoothing with and without prism division. Elements were considered distorted when the interior angles between isoparametric lines was inferior to 45º and superior to 130º.

	Number of distorted elements without prism division	**Number of distorted elements with prism division**
k=0.1	2449	1
k=0.07	8173	1
k=0.05	13569	0
k=0.03	18901	1

3.3 Discussion

Voxel-based meshing is an efficient method for generating patient-specific meshes due to its speed and low complexity. However, it does not represent smooth anatomy with accuracy[16]. Smoothing algorithms can be used to improve the aspect of these meshes but their influence on real anatomical models has never been assessed. Therefore, in this study, the effect of smoothing on the mechanical properties of a voxel mesh of bone was tested.

Apparent Young's modulus was significantly improved by smoothing and converged to the reference value. This is in accordance with previous studies that showed that accuracy of the finite element meshes was improved by smoothing on simple models [16,17]. With smoothing, voxel-based meshes can reach an accuracy equivalent to more complex tetrahedron models. Results achieved with the smooth 32 µm model were comparable to those obtained with the non smooth 16 µm. This would suggest that smoothing allows to reduce the resolution of images and consequently to reduce significantly the number of elements in the mesh. However, effect of smoothing is relevant only for image resolutions where the connection of the trabecula is kept intact. In our case, loss of connection happened at a resolution of 64 µm and explains the large errors found for the Y and Z directions[23]. In these cases, smoothing does not correct errors due to unconnected area. The high dependence on image resolution is one clear limitation of the voxel-based meshes[24] when applied to trabecular structures.

Splitting the distorted elements into prisms improves significantly the quality of the mesh at limited computational costs. In existing voxel mesh software (Simpleware, Simpleware Ltd., Exeter, UK), every element on the surface is unconditionally split into tetrahedral. In our case, elements which are to be split or corrected are discriminated. Hence, the augmentation of elements after division is significantly lower since it only represents a small proportion of elements in the mesh. Moreover, division into prism generates less elements than division into tetrahedra. The fact that improving element quality did not have an influence on result of the analysis may be due to the global aspect of apparent Young's modulus. Local analyses such as surface strain measurements would clearly be more influenced by element quality[24].

This study shows that smoothing offers a real benefit to voxel-based meshes used in micro FE. Further validations with brain and lung images will allow to assess this benefit in the framework of the ContraCancrum project.

4 Application to the brain

In this section, a few examples of the use of the meshing algorithm on brain structures are presented. The aim of these examples is to prove that the process is, in its current form, fitted for the Oncosimulator of the ContraCancrum project.

4.1 Generation of the mesh

The algorithm presented in section 3 was tested on brain images to assess quality of the meshes generated. Since no segmented clinical data of the brain was available at the time where this report was written, the Zubal phantom[25] was used (figure 14). This segmented MRI stack of the brain has dimensions of 256x256x128 bytes. The pixel size in the x,y plane equals 1.1 mm and the resolution in the z axis is 1.4 mm. It offers a first basis to assess the

efficiency of the algorithm. Grey matter and white matter were segmented. Stack was resampled with a factor of 0.5 to generate a model with 115892 elements (including wedge elements). Both no smoothed and smooth models were built. The pass band frequency chosen for the smoothing algorithm was k=0.03. Building the mesh and smoothing took about 2 minutes on a 2.4GHz Pentium 4 personal computer with 2GB of RAM. The model obtained combined the two structures (white and grey matter) separated by a smooth interface.

The smooth mesh presented were constructed in a fully automatic manner. Results show that the external aspect of the mesh is clearly improved by smoothing, even for complex structures such as the brain which bear lots of folds (figure 15 and 16). This is also true for the interface between the tissues (figure 17). The example also proves that the level of automation of the method makes it suitable for the oncosimulator.

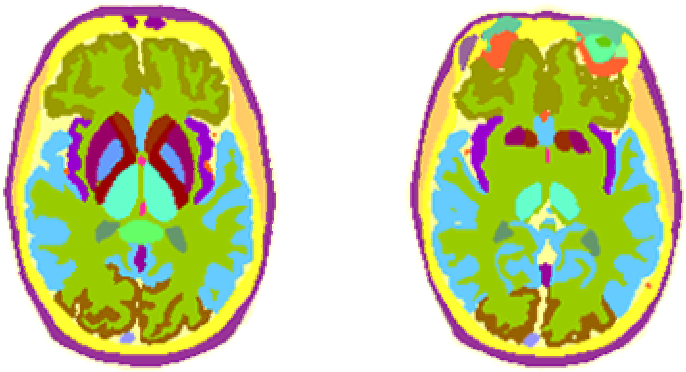

Fig. 14. Sample pictures from the Zubal phantom. Each color corresponds to a segmented anatomical structure in the brain.

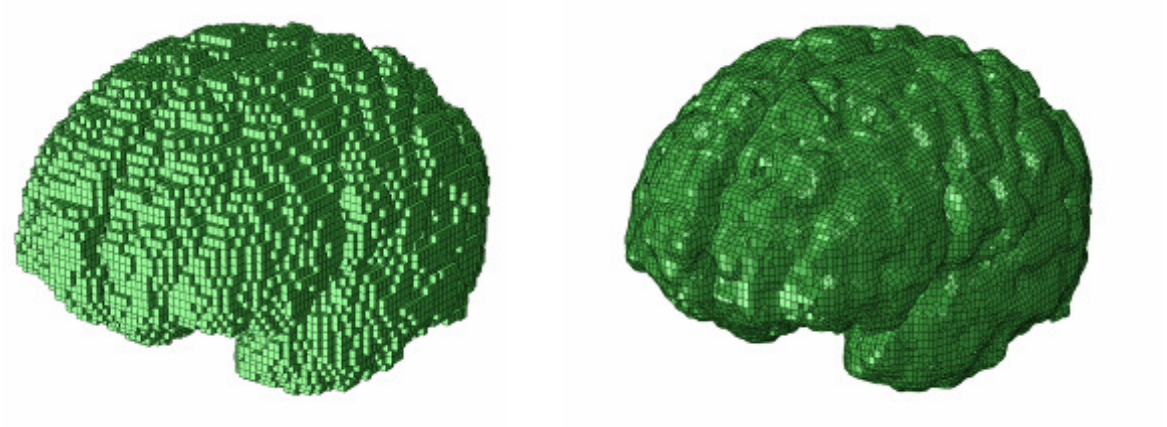

Fig. 15. (Left) voxel mesh of the grey matter obtained from the Zubal phantom. (Right) mesh after smoothing (k=0.03).

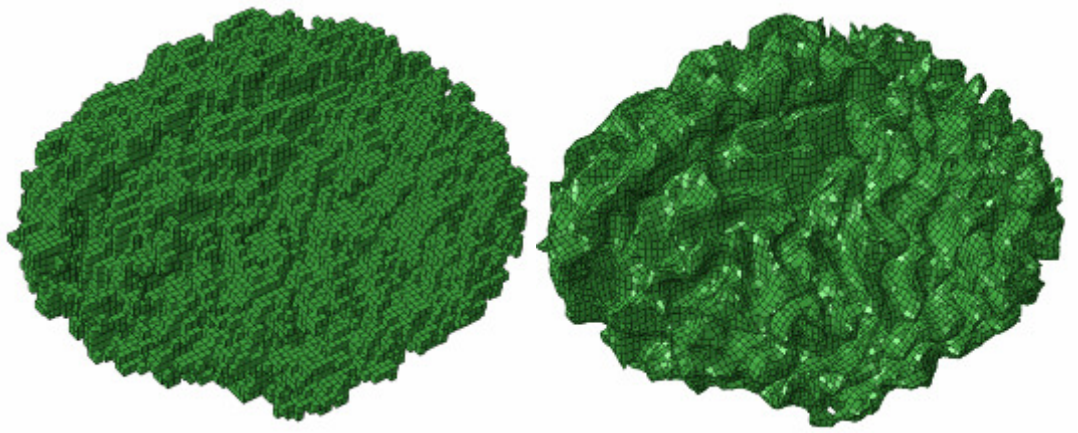

Fig. 16. (Left) voxel mesh of the white matter obtained from the Zubal phantom. (Right) mesh after smoothing (k=0.03). Note that the aspect of the folds is clearly improved with the smoothing.

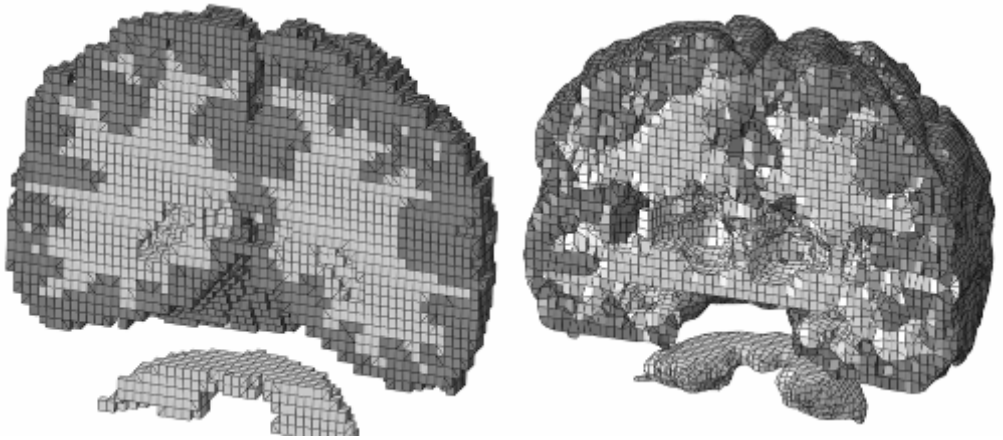

Fig. 17. Interface between the white and grey and white matter (left) without smoothing and (right) enhanced with Taubin smoothing algorithm.

4.2 Simulation of tumour growth

As a preliminary step towards the real use of the algorithm, the growth of a tumour was simulated in the white and grey matter structure presented earlier. A tumour was drawn manually on the segmented MRI of the brain. The meshing algorithm was then applied to generate automatically the model with the white matter, grey matter and the tumour. Raw voxel mesh and smooth voxel mesh were tested. The pass band frequency for the smoothing was set to k=0.03. The material properties of the white and grey matter were set to E=0.694MPa, ν=0.34[26].

The evolution of the tumour was implemented using the user subroutine UMAT in ABAQUS. Constant and uniform internal pressure acting on each node of the tumour at each increment of the analysis was considered. The external surface of the grey matter was fully constrained. Displacement and stresses in the structures surrounding the tumour were calculated (figure 18).

Enhancements of the stress results due to smoothing are clearly visible and underline the accuracy of the method. The stress distribution is more uniform and peaks due to jagged edges are removed (figure 19). This feature is important since stress artificially high would not be realistic when used to drive cells behaviour in the cellular simulator. This example proves that the patient-specific models generated with the presented method are suitable for finite element analysis even for complex structures such as the brain.

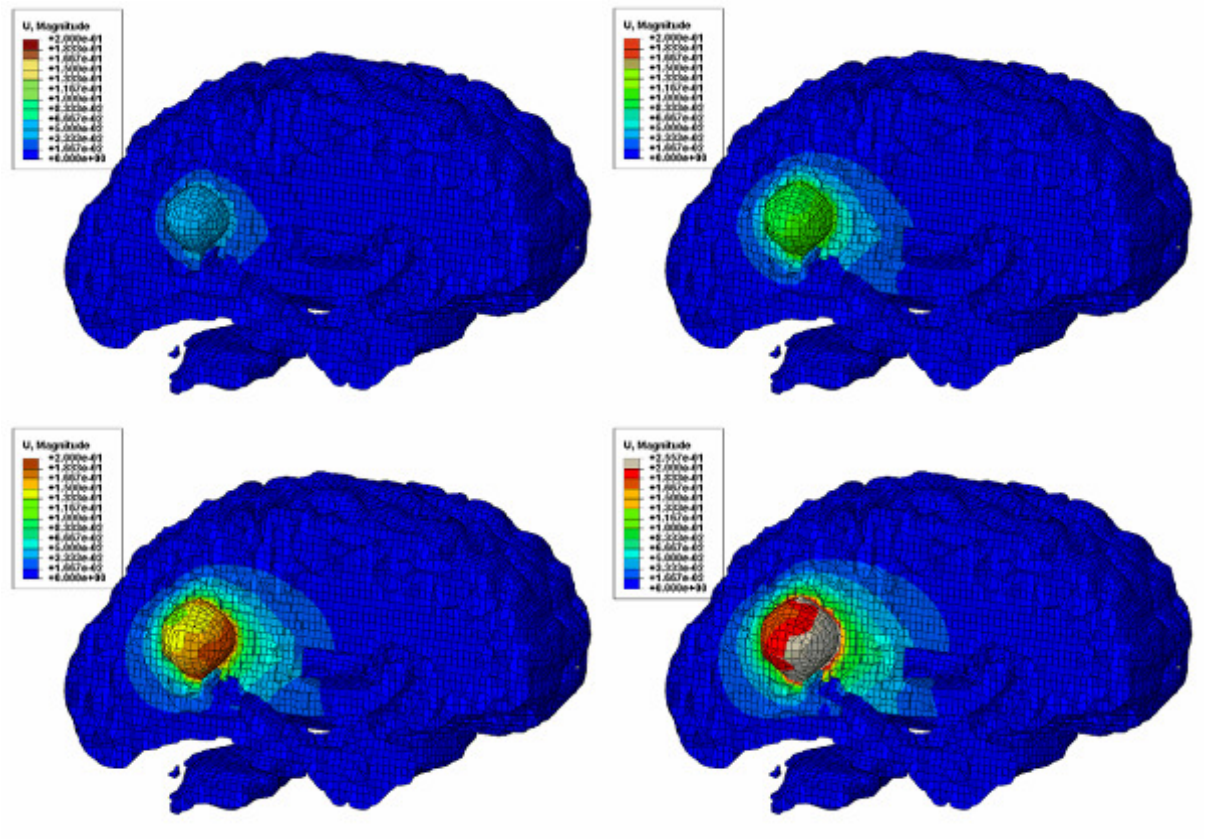

Fig. 18. (From left to right and top to bottom) Simulation of the effect of growth of the tumour on the white and grey matter. The displacement of the nodes is displayed. The size and deformation of the tumour has been voluntarily augmented for visualization.

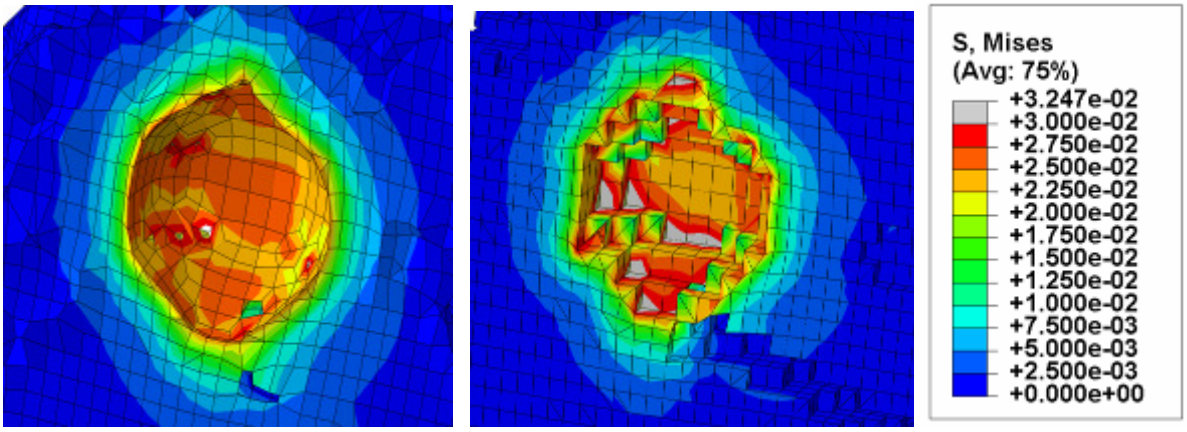

Fig. 19. Mises stresses in the brain structures around the tumour during growth. The distribution of the stresses is clearly more uniform (and thus more realistic) in the smooth (left) case. Jagged edges generate stress peaks at the corner of the elements.

5 Conclusions

5.1 Contributions

In this report, the algorithm used to generate the patient-specific biomechanical model of the oncosimulator was presented. The approach was made as fast and automatic as possible to fulfil the requirements of a clinical application. The voxel mesh approach, which is extremely efficient in terms of time, has been enhanced with a smoothing algorithm which improves its accuracy. Accurate stress information is a priority when designing the model since simulation on cell level will rely on the calculated pressure in the tissues. The algorithm has been assessed by comparing it to a reference model in the framework of bone mechanics. The results of this analysis show that the output of the voxel mesh is significantly improved with the smoothing algorithm and converge to the values given by the reference model. The algorithm has then been tested on a brain MRI and examples demonstrate that the level of automation reached with this method allows to build an accurate biomechanical model without any manual interaction.

5.2 Integration in the Oncosimulator

The algorithm described here is the first step for the biomechanical simulation which will be performed in the oncosimulator (figure 20). It is the link between the output given by the WP7 and the finite element calculation. As for the segmentation, the process needs to be as automatic as possible to guarantee clinical efficiency.

The integration of the meshing in the oncosimulator is processed as following. When a simulation is started for a specific patient, the biomechanical component will connect to the image database and the segmentation of the tissues performed by the image analysis work-package will be retrieved.

Based on the input images, the algorithm described in this report will be used to generate a patient-specific model of the brain/lungs. The process can be performed on remote super computers to ensure fast calculation. As mentioned before, the numbering of the nodes, but also the structure of the program itself can be optimized to decrease time. This optimization will be performed during the preprocessing of the finite element model which will be presented in D6.2. Additionally, depending on the position of the tumour, it might not be useful to mesh the whole brain but just the structures of interest around the tumour. The mesh and boundary conditions will be added to constitute the input model for the biomechanical simulation. Similar to the method described in this report, the settings of these parameters need to be fully automatic. The model generated will be converted from a text file to XML format in order to be solved by the finite element solver chosen for this project. Again, calculation will be performed on remote super computers to increase the speed. Input on local tumour growth and change in volume will be obtained by coupling the biomechanical model to the cellular simulator provided by the WP4. Coupling will be facilitated by the fact that both meshes used by the two simulators are voxel-based. More details on the coupling between the biomechanical simulator and the cellular simulator can be found in the D2.3.

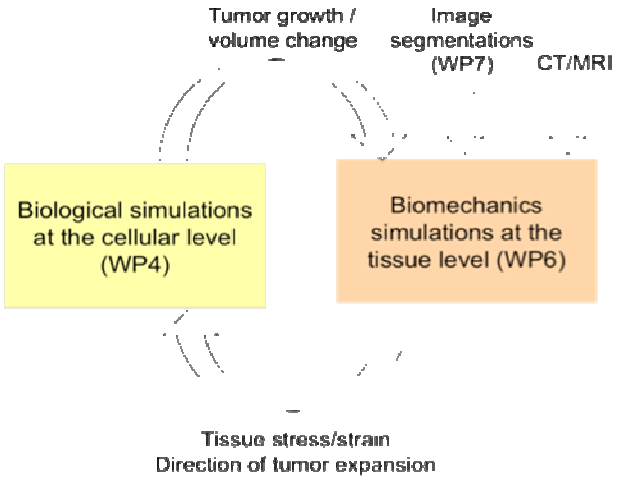

Fig. 20. Workflow of the core structure of the Oncosimulator. The image segmentation provided by the WP 7 is used as an imput to the biomechanical model. Information between the cellular model and the biomechanical model are then exchanged at each step of the simulation.

5.3 Future research and Outlook

As shown by the accuracy study and the examples, this automatic meshing algorithm can, in its current state, be used in the oncosimulator and is suitable for a clinical application. However, some improvements can be made to facilitate the integration. Moreover, automatic generation of patient-specific models is a wide topic and taking research further is possible.

The following section presents future possible milestones in the domain of automatic mesh generation inspired by this project as well as the next steps to be taken for the WP6 in the ContraCancrum project.

5.3.1 Automatic generation of patient-specific mesh

Further improvements of element quality would allow to take smoothing further and improve the accuracy of the mesh. Optimization algorithms could be used but this would be to the detriment of computation time. Another simple solution to this could also be to remove elements with negative volume (as long as their number is small). However, the question rises on what effect will extensive smoothing have on the accuracy of the model, since it might induce the loss of important geometrical features. In that case, a limit would have to be defined for the smoothing.

In regards to the study on accuracy of the patient-specific mesh, future possible research will also consist in comparing mechanical properties of the trabecular bone mesh with real experimental data instead of a virtual model.

5.3.2 In the framework of the ContraCancrum project

When segmented data will be available, a more specific validation of the algorithm in regards to brain and lung structure will be made. The scenario for this validation will be close to the one described in this report for the trabecular structure. A reference model of the anatomy will be built and compared with the smooth voxel mesh presented here. More structures such as skull, ventricles and contours of the tumour (in the case of the brain) will be included.

A study on the accuracy of the segmentation involving several clinicians is planned in WP7. The effect of segmentation variance on biomechanical models will be assessed in parallel. This in order to evaluate the importance of segmentation repeatability on the results of the oncosimulator.

The meshing algorithm need to be integrated in the oncosimulator. This implies implementing and testing it for the super computers that will be used for the ContraCancrum project. This might also include optimization of the algorithm, specific to the type of machine it will be used on. A fully automatic generation of material properties, boundary conditions also has to be implemented to complete the biomechanical model. These steps will be performed in the framework of the D6.2 which aims at calculating stresses and strains in the tissues.

6 Publications

This work has been submitted to:

- the MICCAI Workshop, Computational Biomechanics for Medecine, London, UK, 2009.
- the World Congress for Medical Physics and Biomedical Engineering, Münich, Germany, 2009 (accepted).

References

1. Zienkiewicz OC, Taylor RL. *The finite element method*. 1988.

Ref Type: Book, Whole

2. Mohamed A, Davatzikos C. Finite element modeling of brain tumor mass-effect from 3D medical images. Medical Image Computing and Computer-Assisted Intervention - Miccai 2005, Pt 1 2005; 3749**:** 400-408.

3. Mohamed A, Shen DG, Davatzikos C. Deformable registration of brain tumor images via a statistical model of tumor-induced deformation. Medical Image Computing and Computer-Assisted Intervention - Miccai 2005, Pt 2 2005; 3750**:** 263-270.

4. Kyriacou SK, Davatzikos C, Zinreich SJ, Bryan RN. Nonlinear elastic registration of brain images with tumor pathology using a biomechanical model. Ieee Transactions on Medical Imaging 1999; 18**:** 580-592.

5. Wasserman R, Acharya R, Sibata C, Shin KH. A patient-specific in vivo tumor model. Mathematical Biosciences 1996; 136**:** 111-140.

6. Angelini ED, Clatz O, Mandonnet E, Konukoglu E, Capelle L, Duffau H. Glioma dynamics and computational models: a review of segmentation, registration, and in silico growth algorithms and their clinical applications. Current Medical Imaging Reviews 2007; 3**:** 262-276.

7. Viceconti M, Davinelli M, Taddei F, Cappello A. Automatic generation of accurate subject-specific bone finite element models to be used in clinical studies. Journal of Biomechanics 2004; 37**:** 1597-1605.

8. Viceconti M, Taddei F. Automatic generation of finite element meshes from computed tomography data. Crit Rev Biomed Eng 2003; 31**:** 27-72.

9. Helgason B, Perilli E, Schileo E, Taddei F, Brynjolfsson S, Viceconti M. Mathematical relationships between bone density and mechanical properties: a literature review. Clin Biomech (Bristol , Avon) 2008; 23**:** 135-146.

10. Bossard, P. L., MArtz, H. E., and Hollerbach, K. Finite element analysis of human joints: image processing and meshing issues. UCRL-JC-126079. 1996. Livermore, California, Lawrence Livermore National Laboratory.

Ref Type: Report

11. Schneiders, R. Automatic generation of hexahedral finite element meshes. 103-114. 1995. Albuquerque, New Mexico, Sandia National Laboratories. 4th International Meshing Roundtable.

Ref Type: Conference Proceeding

12. Keyak JH, Meagher JM, Skinner HB, Mote CD. Automated 3-Dimensional Finite-Element Modeling of Bone - A New Method. Journal of Biomedical Engineering 1990; 12**:** 389-397.

13. Keyak JH, Skinner HB. 3-Dimensional Finite-Element Modeling of Bone - Effects of Element Size. Journal of Biomedical Engineering 1992; 14**:** 483-489.

14. Keyak JH, Fourkas MG, Meagher JM, Skinner HB. Validation of An Automated-Method of 3-Dimensional Finite-Element Modeling of Bone. Journal of Biomedical Engineering 1993; 15**:** 505-509.

15. Hollister, S. J. and Riemer, B. A. Digital image based finite element analysis for bone microstructure using conjugate gradient and Gaussian filter technique. 1993. Mathematical Methods in Medical Imaging II: SPIE.

Ref Type: Conference Proceeding

16. Boyd SK, Muller R. Smooth surface meshing for automated finite element model generation from 3D image data. Journal of Biomechanics 2006; 39**:** 1287-1295.

17. Camacho DLA, Hopper RH, Lin GM, Myers BS. An improved method for finite element mesh generation of geometrically complex structures with application to the skullbase. Journal of Biomechanics 1997; 30**:** 1067-1070.

18. Merz B, Niederer P, Muller R, Ruegsegger P. Automated finite element analysis of excised human femora based on precision-QCT. Journal of Biomechanical Engineering-Transactions of the Asme 1996; 118**:** 387-390.

19. Ohtake Y, Belyaev A, Bogaevski I. Mesh regularization and adaptive smoothing. Computer-Aided Design 2001; 33**:** 789-800.

20. Taubin, G. A signal processing approach to fair surface design. 351-358. 1995. Computer Graphics.

Ref Type: Conference Proceeding

21. Zhang YJ, Bajaj C, Xu GL. Surface smoothing and quality improvement of quadrilateral/hexahedral meshes with geometric flow. Communications in Numerical Methods in Engineering 2009; 25**:** 1-18.

22. Schroeder W, Martin K, Lorensen B. *The Visualization Toolkit: an object-oriented approach to 3D graphics, 4th edition*. Kitware Inc. publishers, 2009.

Ref Type: Book, Whole

23. Ulrich D, van Rietbergen B, Weinans H, Ruegsegger P. Finite element analysis of trabecular bone structure: a comparison of image-based meshing techniques. Journal of Biomechanics 1998; 31**:** 1187-1192.

24. Viceconti M, Bellingeri L, Cristofolini L, Toni A. A comparative study on different methods of automatic mesh generation of human femurs. Medical Engineering & Physics 1998; 20**:** 1-10.

25. Zubal IG, Harrell CR, Smith EO, Rattner Z, Gindi G, Hoffer PB. Computerized 3-Dimensional Segmented Human Anatomy. Medical Physics 1994; 21**:** 299-302.

26. Clatz O, Delingette H, Bardinet E, Dormont D, Ayache N. Patient-specific biomechanical model of the brain: Application to Parkinson's disease procedure. Surgery Simulation and Soft Tissue Modeling, Proceedings 2003; 2673**:** 321-331.